Journal of the European Ceramic Society 22 (2002) 2543–2549
www.elsevier.com/locate/jeurceramsoc

Characterisation and high temperature mechanical properties of zirconium boride-based materials

J.J. Meléndez-Martínez[a,*], A. Domínguez-Rodríguez[a], F. Monteverde[b], C. Melandri[b], G. de Portu[b]

[a]*Department de Física de la Materia Condensada, University of Seville, Box 1065, 41080 Seville, Spain*
[b]*CNR, Research Institute for Ceramics Technology (IRTEC), Faenza, Italy*

Received 10 October 2001; received in revised form 1 February 2002; accepted 20 February 2002

Abstract

Two different ZrB_2-based materials were produced by hot pressing: pure ZrB_2 and $ZrB_2 + 4$wt.% Ni. The relative densities of the two materials were 86.5 and 98.0%, respectively. Several physical and mechanical properties were measured in ambient air. From these data it appears that the porosity of 13.5% of pure ZrB_2 strongly affects the properties. However at high temperature the presence of Ni-rich phases dominates the fracture behaviour and is responsible for the dramatic strength degradation (especially at 1200 °C). The high temperature creep was evaluated by uniaxial compression tests. Samples of both materials were deformed in argon atmosphere at temperatures between 1400 and 1600 °C and at stresses ranging between 47.0 and 472.3 MPa (pure ZrB_2) and 10–63.5 MPa (Ni-doped ZrB_2). Pure ZrB_2 showed a ductile behaviour under these conditions. On the other hand, Ni-doped ZrB_2 failed catastrophically for stresses higher than 25 MPa, approximately, at relatively low strains, showing a ductile behaviour only at lower stresses. This behaviour may be related to the presence of Ni-rich grain boundary phases at triple points of the grain structure.

Keywords: Mechanical properties; Microstructure; Processing; Zirconium boride

1. Introduction

Zirconium diboride (ZrB_2) ceramics have a high melting point, high hardness, high electrical conductivity, excellent corrosion resistance against molten iron and slags, superb thermal shock resistance. It is one of the promising materials for high temperature applications in several industrial sectors, such as foundry or refractory industries. Like TiB_2, ZrB_2 is wet by molten metals but is not attacked by them, making it a useful material for molten metal crucibles, thermowell tubes for steel refining and in electrical devices: heaters and igniters.[1] Applications are also found in aerospatial industry: hypersonic re-entry vehicles, leading edges, nose caps, rocket nozzle inserts and air augmented propulsion systems components.[1–4]

The densification of pure ZrB_2 is complicated by two characteristics of this compound, similar to other transition metal borides: the high melting point and the comparatively high vapour pressure of the constituents. Therefore, relatively high densities are achieved only by hot pressing at temperatures higher than 1900 °C.[1,5] As for TiB_2 materials,[6] the introduction of sintering aids like Fe, Ni, Co, W, C, WC improves the final density and allows to lower the densification temperature.[1,7] Attempts to densify ZrB_2 without sintering aids or with the addition of boron resulted in rather low final densities.[8] Among the possibilities of the electroconductive monolithic or composite ZrB_2-based ceramics, the possibility to machine them by electrical discharge offers a powerful tool to manufacture complex shaped components.[9–12]

The properties of the dense ZrB_2-based materials become strictly dependent on the starting powders and processing parameters as they determine microstructure: grain size, porosity, volume and chemistry of the secondary phases, etc.

* Corresponding author. Tel.: +34-95-455-0964; fax: +34-95-461-2097.
E-mail address: melendez@unex.es (J.J. Meléndez-Martínez).

0955-2219/02/$ - see front matter
PII: S0955-2219(02)00114-0

This work attempts to highlight the influence of the starting composition on the high temperature mechanical properties of ZrB_2-based ceramics, obtained from fine commercial powders.

2. Experimental procedure

ZrB_2 powder produced by H.C. Starck (Germany) was selected as raw material. This powder has a specific surface area of 1 m^2/g, and particle size ranges from 0.5 to about 8 μm. The particle shape is irregular and mainly acicular. Oxygen content, measured by LECO is 1 wt.%. Other impurities are (wt.%): C 0.25, N 0.25, Fe 0.1, Hf 0.2.

Two different materials were produced:

material A: from the as produced ZrB_2 powder, by hot pressing at 1900 °C (the maximum temperature allowed by our equipment) for 30 min with the applied pressure of 30 MPa;
material B: from the powder mixture $ZrB_2 + 4$ wt.% Ni, by hot pressing at 1850 °C for 30 min and with the applied pressure of 30 MPa.

The following mechanical properties were measured (Table 1): elastic modulus (E) by the resonance frequency method on samples of dimensions $28.0\times8.0\times0.8$ mm^3, 4-pt. flexural strength (S) in ambient air, from room temperature up to 1400 °C, on $25.0\times2.5\times2.0$ mm^3 test bars, using outer span of 40 mm, inner span of 20 mm, crosshead speed of 0.5 mm/min; microhardness (Hv1.0) by a Vickers indenter, applied load 1 kg; fracture toughness (K_{IC}) using two methods: (1) direct crack measurement (DCM)[13] with a load of 10 kg, (2) chevron notched beam method (CNB)[14] on $25.0\times2.5\times2.0$ mm^3 bars.

Compressive creep tests were performed in controlled argon atmosphere at 1400, 1500 and 1600 °C and at stresses ranging between 47.0 and 472.3 MPa (for material A) and 31.8 and 63.5 MPa (for material B) on parallelepipedical samples of dimensions $5\times2.5\times2.5$ mm^3. The tests were carried out in a prototype deadweight load device described elsewhere.[15]

The microstructure of the as-processed materials and of the crept samples was analysed by scanning electron microscopy and EDX analyser on polished and on fracture surfaces. Crystalline phases were identified by X-ray diffraction analyses.

3. Results and discussion

3.1. Microstructure

The final density of the material without sintering aids (A) is 5.28 g/cm^3, corresponding to a relative density of 86.5%. The only crystalline phase is ZrB_2. The microstructure of a fracture surface of the material reveals the presence of porosity and that the intra-granular fracture mode is dominant (Fig. 1).

On the contrary, material B, produced with the addition of Ni as sintering aid, reached higher final density: 6.05 g/cm^3 (i.e. 98.0%). The presence of Ni promotes the formation of liquid phase at high temperature, similarly to the phenomena observed during the sintering of TiB_2 [6] and in agreement with previous results on the effects of the addition of Fe to ZrB_2.[7] The densification of mixture B in fact started at about 1260 °C (while that of material A started at 1750 °C). The mechanisms of sintering activation by doping is not yet readily understood but an increase of volume diffusion and a retardation of evaporation seems to be likely. In the hot pressed material, Ni-rich secondary grain boundary phases (metal Ni and Ni-B compounds) are located mainly at triple points (Fig. 2 a–c). It has to be pointed out that, in the back scattered electron images of Fig. 2b and c, the contrast associated to the ZrB_2 grains arises from the channeling of the accelerated electrons impinging the randomly oriented ZrB_2 crystals and not from changes of the mean atomic number (i.e. of the phase stoichiometry).

From X-ray diffraction analyses, traces of Ni_2B were identified, and, by EDX analyses, areas containing only pure Ni were found. Also grain boundaries without secondary phases exist among ZrB_2 grains.

Secondary ion mass spectrometry (SIMS) analyses, reported elsewhere,[16] evidenced phases in the systems Zr–B–O, Ni–B, Zr–Ni–O, Zr–O, indicating reactivity

Table 1
Values of the mechanical properties of the two hot pressed ZrB_2 based ceramics

Material	E (GPa)	HV (GPa)	K_{IC} (MPa·$m^{1/2}$)		S (MPa)					
			DCM	CNB	RT	600 °C	800 °C	1000 °C	1200 °C	1400 °C
A	346	8.7±0.4	3.5±0.3	2.35±0.15	351±31	–	342±42	317±57	312±11	219±7
B	496	14.4±0.8	2.8±0.3	3.4 ±0.4	371±24	618±8	624±37	237±3	15±1	–

E, Young's modulus; HV, Vickers Hardness; K_{IC}, Fracture toughness; S, flexural strength; DCM, direct crack measurement; CNB, chevron notched beam method.

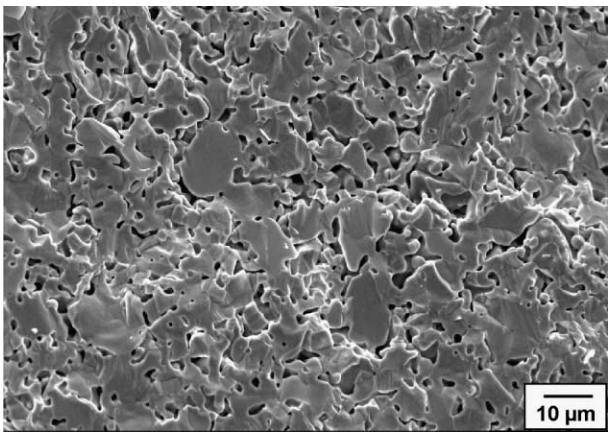

Fig. 1. Fracture surface of sample A, showing a dominant intragranular fracture mode.

between the different element during hot pressing. This assumption is substantiated by small intergranular ZrO_2 particles, evidenced in Fig. 2b and c. Moreover, Zr–O compounds are also present in the spherical inclusions distributed mainly at grain boundaries (Fig. 3). Energy dispersive X-ray analysis (EDX) revealed that inner featuers of these inclusions are constituted by zirconium oxide small particles embedded in a glassy phase containing B, O, Zr and low amounts of impurities (i.e. Al, Si). It can be assumed that the glass formed at high temperature as a consequence of oxygen distributed on the surface of zirconium diboride particles, then other impurities segregated in this glass. During cooling from the hot pressing temperature, zirconium oxide particles precipitated inside the glassy inclusions.[17]

3.2. Mechanical and physical properties

The values of the measured properties are summarised in Table 1. The value of Young's modulus measured on sample A is much lower than the values reported in literature (440–460 GPa)[1] due to the high amount of porosity, while the value measured on sample B is very high. Residual porosity also affects hardness in material A; material B has an higher hardness, the values fall in the large range reported in literature.[1,11]

Fracture toughness measurements, obtained by two different methods, give different results. In material A, due to the porosity, DCM method results in higher values than CNB method. In the case of material B, relatively low values result from DCM method. Fig. 4 reveals that the DCM method is not suitable to measure toughness, as the cracks propagate in direction different

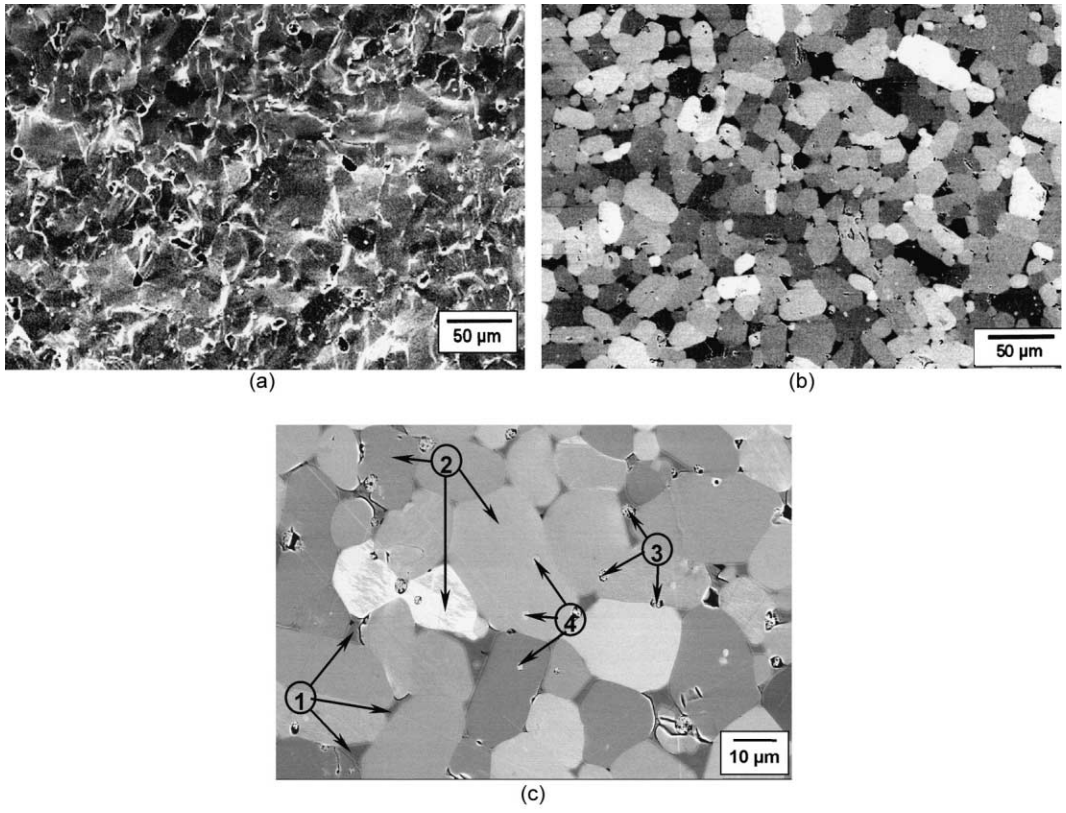

Fig. 2. Microstructural features of the material densified with the addition of 4 wt.% of Ni. (a) Fracture surface (secondary electron image). (b) Back scattered electron image of the polished surface. In Fig. 2(c), the following features are marked: 1: Ni-rich grain boundary phase; 2: ZrB_2 grains; 3: ZrO_2 nanoparticles embedded in a glassy phase containing B, O, Zr, and impurities; 4: ZrO_2 particles.

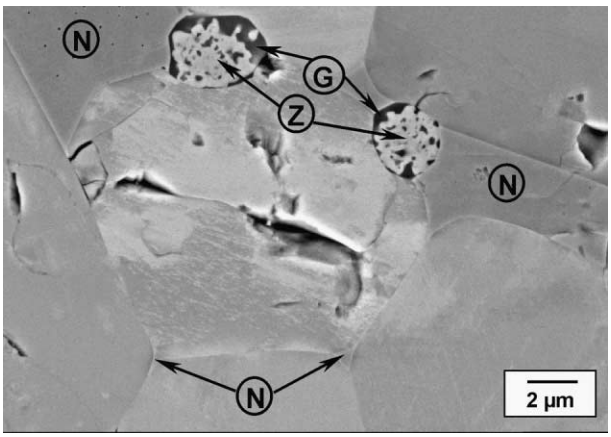

Fig. 3. Back scattered electron image that highlights both Ni-rich grain boundary phase (labelled N) and the spherical glassy inclusion (labelled G) containing clusters of ZrO_2 nanoprecipitates (labelled Z).

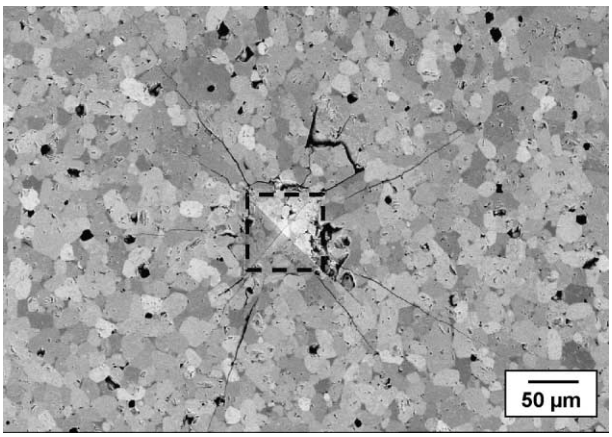

Fig. 4. Back scattered electron image of a Vickers indentation (marked with a dashed square) and the consequent crack propagation on a polished surface of the Ni-doped sample.

from the behaviour foreseen by the model; crack propagation is mostly intra-granular and typical of low toughness materials.

Strength variation with temperature is shown in Fig. 5. In material A, strength (about 350 MPa) is almost constant up to about 1200 °C and then the decrease is rather low; at 1400 °C it is still higher than 200 MPa. These values are higher than those reported in literature for ZrB_2-based materials.[1,18,19] On the contrary, material B shows an improved strength in the temperature range 600–800 °C, reaching values higher than 600 MPa, that are excellent for this class of materials. A strong strength degradation occurs at 1000 °C and particularly at 1200 °C. This behaviour can be attributed to different effects dependent on the grain boundary phases of material B. A partial and progressive softening of the Ni-based grain boundary phases induces a strengthening effect at intermediate temperatures (i.e. 600–800 °C), due to the crack tip blunting. If this mechanism is dominant in competing with those related to crack propagation, an increase in strength can be observed. With our experimental conditions it is possible that the weakening mechanisms associated to the high tempeartures, do not have time to occur before fracturing up to 800 °C. Above 800 °C, when the viscosity of the grain boundary phases lowers (in particular between 1000 and

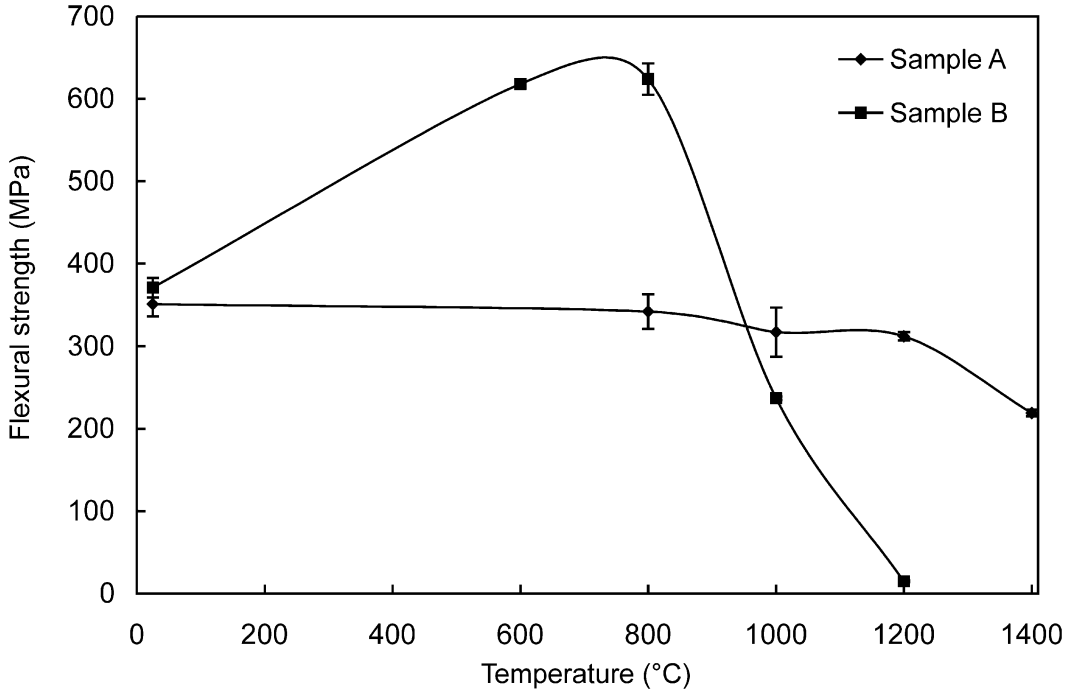

Fig. 5. Plot showing the variation of the flexural strength in function of the test temperature, for both the materials: A undoped, B: Ni-doped.

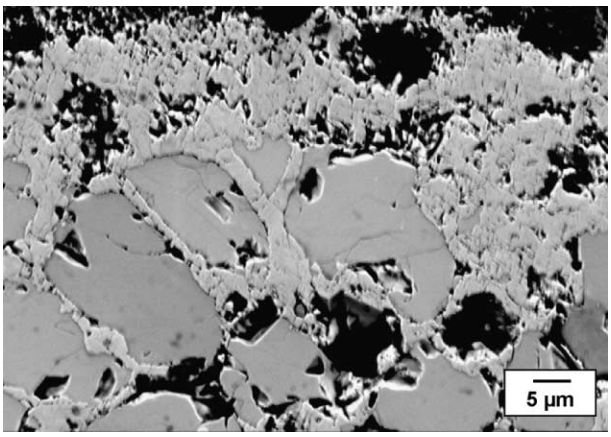

Fig. 6. Back scattered electron image of the polished cross section of sample B, oxidised at 1000 °C for 1 h. Oxidation propagating along grain boundary and subsequent material degradation are evidenced.

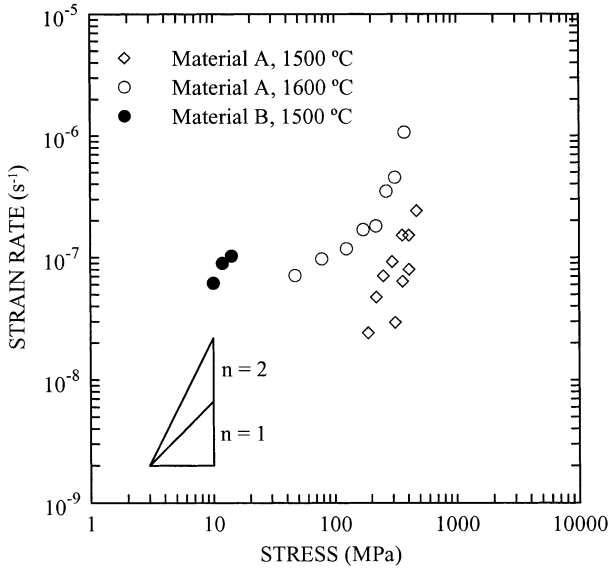

Fig. 7. ln $\dot{\varepsilon}$ vs. ln σ curves for undoped and Ni-doped ZrB_2 at 1500 °C and 1600 °C. The slope of the best-fit straight lines is equal to the stress exponent.

1200 °C), the weakening mechanisms start to be more effective and the rupture occurs at very low loads. A similar phenomenon has been already reported in literature.[20,21] An additional effect can be ascribed to the surface oxidation, as these tests are carried out in air. In fact, after a thermal cycle at 1000 °C for 1 h in air, the surface and subsurface degradation is evident (fig. 6): primarily oxygen attacks grain boundary phases, then the oxidation of ZrB_2 grains occurs.[17] The disappearance of the grain boundary phase, the formation of oxides with a consequent volume increase contribute to create defects and cracks at grain boundaries that progressively propagate towards the bulk material and induce the strong strength degradation.

Nevertheless, the oxidation effect in material B has been demonstrated to be secondary by creep experiments (see later), since the failure at very low stresses takes place even when the atmosphere is not oxidising.

On the contrary, in the case of material A, the oxidation induces the formation of a surface oxide layer. At grain boundaries, where oxygen penetrates through interconnected porosity, only some zirconium oxide particles form, but they do not induce catastrophic degradation of the material structure.[17] In fact, the rigid skeleton of the ZrB_2 grains maintains its original configuration, therefore good strength values are measured up to 1400 °C.

3.3. Creep behaviour

Material A showed a high creep resistance under the testing conditions of temperature and applied stress. At 1400 °C, a strain rate of $\sim 6 \cdot 10^{-8}$ s^{-1} was measured under $\sigma = 298$ MPa: below this value, no deformation was measured within the experimental accuracy. At 1500 °C, strain rates close to 10^{-7} s^{-1} were obtained under stresses between 298 and 408 MPa; finally, at 1600 °C, a strain rate close to $2 \cdot 10^{-7}$ s^{-1} was obtained under $\sigma = 220$ MPa.

The results were analysed in terms of the Norton potential law:

$$\dot{\varepsilon} = A(T)\sigma^n$$

where $\dot{\varepsilon}$ is the steady strain rate, σ is the applied stress, A is a constant (but dependent on the temperature) and n is the stress exponent. The tests performed at 1500 °C yielded an average value of $n = 1.7$. At 1600 °C, a value of $n = 0.6$ was obtained at stresses below ~220 MPa. Above this value, accelerated creep occurred, leading to the failure of the testing sample at $\varepsilon \sim 8.5\%$.

Material B was tested at 1400 and 1500 °C. At the lowest temperature, the testing sample failed catastrophically after loading, at a stress of 63.5 MPa, as also occurred at 1500 °C under an applied stress of 39.8 MPa. From creep tests carried out at lower stresses (between 10 and 20 MPa, approximately), a value $n = 1.5$ of the stress exponent was found.

Fig. 7 summarises the creep behaviour of the pure and doped materials. The creep results are consistent with the mechanical properties listed in Table 1. Thus, the high creep resistance of material A agrees with its high strength at high temperatures; on the other hand, the strength degradation at 1200 °C showed by material B results in its poor creep resistance. As this degradation occurred even when the tests were conducted in controlled reducer atmosphere, the degradation mechanism related to the oxidation of material B should be considered as secondary.

The microstructure of the crept samples was found to be similar to that of as-processed materials. In particular, no densification processes were expected, since the creep temperatures were much lower than the hot-pressing temperatures.

The complete correlation between the strength and fracture toughness values and the creep properties for both materials is a very difficult task and needs more experimental data. Besides, the creep mechanisms are unknown as well. Therefore, a further investigation of the mechanical properties at high temperatures of pure and Ni-doped ZrB_2 is necessary. This study is now in progress at the University of Seville.

4. Conclusions

Zirconium diboride-based ceramics, densified without additives and with the addition of 4 wt.% of Ni exhibit different microstructure and properties. Hardness, toughness and Young's modulus at room temperature are remarkably higher in the Ni-doped material, mainly due to the higher relative density (about 98%) and to the presence of ductile, Ni-rich, secondary phases. However, this material show a strong strength decrease at temperatures higher than about 1000 °C. This could be due to that:

1. the Ni-rich grain boundary phases start to melt at temperature above 800 °C. The softening of these phases increase rapidly with the temperature, leading to catastrophic failure at temperatures higher than about 1000 °C even at low stresses.
2. these Ni-rich grain boundary phases easily react with oxygen, enhancing the oxidation propagation towards the bulk along the grain boundaries, thus creating defects and material degradation. This mechanisms should be considered as secondary.
3. the glassy inclusions melt, offer easier paths for the inward diffusion of oxygen towards the material's bulk enhancing oxidation of the ZrB_2 skeleton; for temperatures >800 °C, it may vaporise leaving voids and cracks;

Notwithstanding the residual porosity (about 13%) the undoped material maintained a constant flexural strength up to 1400 °C.

The creep behaviour of both materials is in good agreement with their mechanical properties. Thus, the undoped material showed a high creep resistance, whereas the strength degradation characteristic of Ni-doped material resulted in poor creep properties. A further study is necessary to identify the creep mechanisms for both materials.

Acknowledgements

The activity carried out at IRTEC was supported by ASI (Agenzia Spaziale Italiana), Project NEIN700257.

References

1. Mroz, C., Annual mineral review. Zirconium diboride. *Am. Ceram. Soc. Bull.*, 1995, **74**, 165–166.
2. Low, I. M. and McPherson, R., Fabrication of new zirconium boride ceramics. *J. Mat. Sci. Lett.*, 1989, **8**, 1281–1283.
3. Upadhya, K., Yang, J. M. and Hoffmann, W. P., Materials for ultrahigh temperature structural applications. *Am. Ceram. Soc. Bull*, 1997, **58**, 51–56.
4. Van de Goor, G., Sagesser, P. and Berroth, K., Electrically conductive ceramic composites. In *Advanced Multilayered and Fibre-Reinforced Composites*, ed. Y. M. Haddad. Kluwer Academic Publishers, The Netherlands, 1998, pp. 311–322.
5. Hayami, R., Iwasa, M. and Kinoshita, M., Effects of applied pressure on hot pressing of ZrB_2. *Yogyo-Kyokai-Shi*, 1978, **88**, 352–359.
6. Bellosi, A., and Monteverde, F. Microstructure and properties of titanium nitride and titanium boride-based ceramics. In *Key Engineering Materials*, Vols. 175–176. Trans Tech Publications, 2000, pp. 130–139.
7. Woo, S.-K., Han, I.-S., Kang, H.-S., Yang, J.-H. and Kim, C.-H., Sintering of zirconium diboride through Fe-based liquids phases. *J. Korean Ceram. Soc.*, 1996, **33**, 259–262.
8. Øvreb", D. N., Riley, F. L., Densification of zirconium diboride. In *Sixth—ECerS Conference & Exhibition", Extended Abstract Vol 2.*, IOM Communications Ltd, University Press, Cambridge, UK, 1999, pp. 19–20.
9. Jimbou, R., Takahashi, K., Matsushita, Y. and Kosugi, T., SiC–ZrB_2 electroconductive ceramic composite. *Adv. Cer. Mat*, 1986, **1**, 341–346.
10. Nakamura, M., Shigematsu, I., Kanayama, K. and Hirai, Y., Surface damage in ZrB_2-based composite ceramics induced by electro-discharge machining. *J. Mat. Sci.*, 1991, **26**, 6078–6082.
11. Schuldies, J. J. and Branch, J. A., Ceramic composites: emerging processes, applications. *Ceram. Ind.*, 1992, **138**, 43–46.
12. Cheng, Y. M., Eubank, P. T. and Gadalla, A. M., Electrical discharge machning of ZrB_2-based ceramics. *Mater. Manuf. Processes*, 1996, **11**, 565–574.
13. Anstis, G. R., Chantikul, P., Lawn, B. R. and Marshall, D. B., A critical evaluation of indentation techniques for measuring fracture toughness: I, direct crack measurements. *J. Am. Ceram. Soc.*, 1981, **64**, 533–538.
14. Munz, D. G., Shannon, J. L. Jr. and Bubsey, R. T., Fracture toughness calculation from maximum load in four point bend tests of Chevron Notch specimens. *Int. J. of Fracture*, 1980, **16**, R137–R141.
15. Gervais, H., Pellicier, B. and Castaing, J., Machine de fluage pour essais en compresión à hautes températures de matériaux céramiques. *Rev. Int. Hautes Temp. Refract.*, 1978, **15**, 43.
16. Daolio, S., Fabrizio, M., Piccirillo, C., Muolo, M. L., Passerone, A. and Bellosi, A., Secondary ion mass spectrometry in the characterisation of boron-based ceramics. *Rapid Commun. Mass Spectrom*, 2001, **15**, 1–7.
17. Bellosi, A., Monteverde, F., Dalle Fabbriche, D., Melandri, C., Microstructure and properties of ZrB_2-based ceramics. *Journal of Materials Processing and Manufacturing Science* (submitted for publication).

18. Zhong, X. and Zao, H., High temperature properties of refractory composites. *Am. Ceram. Soc. Bull.*, 1999, **60**, 98–101.
19. Strauss, E. L. and Kiefer, T. F., Strength of zirconium diboride ceramics after cyclic loading or heating. *J. Am. Ceram. Soc.*, 1975, **58**, 399–401.
20. Evans, A. G. and Wiederhorn, S. M., Crack propagation and failure prediction in Si3N4 at elevated temperatures. *J. Mat. Science*, 1974, **9**(2), 270–278.
21. Knickerbocker, S. H., Zangvil, A. and Brown, S. D., Displacement rate and tempearture effects in fracture of a hot-pressed silicon nitride at 1100 °C to 1325. *J. Am. Ceram. Soc.*, 1984, **67**(5), 365–368.